ARTICLE

Connectomic Determinants of Subcallosal Cingulate Deep Brain Stimulation for Depression

Ha Neul Song, M.S.,[1] Ki Sueng Choi, Ph.D.,[1] Brian H. Kopell, M.D.,[2] Martijn Figee, M.D., Ph.D.,[1] Jip de Bruin, M.S.,[1] Jungho Cha, Ph.D.,[1] Patricio Riva-Posse, M.D.,[3] Alexandre Boutet, M.D., Ph.D.,[4] Gavin Elias, M.D., Ph.D.,[5] Jurgen Germann, Ph.D.,[5,6] Sidney H. Kennedy, M.D.,[7] Lyndahl Himes, Ph.D.,[8] Robert E. Gross, M.D., Ph.D.,[9] Andres M. Lozano, M.D., Ph.D.,[10] Binith Cheeran, M.D., Ph.D.,[8] Helen S. Mayberg, M.D.[1]

Objective: Subcallosal cingulate (SCC) deep brain stimulation (DBS) has shown promise for treatment-resistant depression. This study retrospectively evaluated a large curated SCC-DBS dataset to identify connectomic factors associated with sustained clinical improvement across patients, focusing on the white matter bundles consistently implicated in patient-specific connectome-based targeting.

Methods: A total of 131 patients (mean age=46.67 years, SD=9.79; 60.31% female) with treatment-resistant depression from three independent cohorts received bilateral SCC-DBS using site-specific targeting methods. Clinical improvements were assessed using the 17-item Hamilton Depression Rating Scale (HAM-D). Based on individual DBS settings, volumes of tissue activated were reconstructed, and voxel-wise stimulation mapping and normative fiber-wise analyses were performed to assess contributions of white matter bundles to therapeutic response.

Results: Responders (patients with ≥50% reduction in HAM-D score) exhibited a less variable spatial distribution of volumes of tissue activated than nonresponders. Probabilistic stimulation mapping identified a focal cluster associated with clinical improvement. Fiber-wise analyses showed that stimulation of predefined white matter tracts targeted by connectome-based SCC-DBS contributed to clinical efficacy. Notably, failure to activate the left cingulum bundle and medial uncinate fasciculus decreased the therapeutic effects of SCC-DBS.

Conclusions: This study highlights the significance of stimulating critical white matter bundles for effective SCC-DBS. Available evidence supports the idea that precisely targeting the lateralized cingulum bundle and medial uncinate fasciculus is essential for sustained clinical improvement. These findings suggest potential advantages of connectome-based targeting for SCC-DBS over targeting based solely on anatomical landmarks or normative atlases, using a method that is precise, reliable, and scalable for future use in individual patients.

Am J Psychiatry 2026; 183:764–774; doi: 10.1176/appi.ajp.20250449

Major depressive disorder (MDD) is highly prevalent, affecting approximately 6% of the global population annually and one in six adults over their lifetime (1). While first-line treatments, including psychotherapy and pharmacotherapy, are effective for many, approximately 30% of patients develop treatment-resistant depression (2–4). Deep brain stimulation (DBS), a surgical neuromodulatory therapy, is a potential strategy for patients who have not improved after several treatment approaches. DBS delivers chronic high-frequency electrical stimulation to modulate abnormal regional and circuit-level brain activity (5–9). Multiple reports and meta-analyses (5, 10–18) indicate that DBS of the subcallosal cingulate cortex (SCC), first piloted in 2005, has demonstrated significant and sustained antidepressant effects, although results have been variable across studies. Sources of this variance include, but are not limited to, patient selection, study design, and surgical targeting methods. Methods to accurately and precisely define the target, as with all DBS indications, are a critical and controllable variable, and are the focus of this study.

Selection of the target for delivery of DBS is grounded in the premise that depression is a multiregion network disorder organized by patterns of functional and structural connectivity (11, 19–23). The SCC, an anchor member of the limbic network and a primary site of change with various antidepressant treatments (10, 11, 24–27), is also notable for its direct structural connections to several hub regions in the salience (anterior insula, dorsal anterior cingulate), default mode (ventral medial prefrontal cortex, posterior cingulate cortex, hippocampus), and action mode (mid-cingulate) networks via the cingulum bundle (CB), forceps minor (FM), uncinate fasciculus, and frontostriatal bundle (25, 28–38).

This understanding has driven a shift from anatomical landmark–based to connectome-based SCC-DBS targeting, with the aim of modulating white matter (WM) bundles and their projections to cortical and subcortical regions and associated networks implicated in the pathophysiology of depression (6, 11, 34, 35, 39, 40). Notably, a patient-specific connectomic approach has enhanced clinical outcomes of SCC-DBS in open-label studies, suggesting the importance of precise WM recruitment in alleviating symptoms in treatment-resistant depression (34, 35, 40–42).

The connectome-based targeting method for SCC-DBS, which has evolved and subsequently been refined with the addition of individual tractography profiles of new responders (34), aims to maximize the stimulation of the critical WM bundles connected to the SCC (34, 43). However, the role of specific WM recruitment in SCC-DBS efficacy is incompletely understood. Small sample sizes and qualitative analyses have limited the existing evidence supporting WM activation in SCC-DBS (29–31, 34, 41). Furthermore, the differential contributions of specific WM bundles to clinical outcomes and their relationship to long-term efficacy remain underexplored (44).

To address these gaps, we analyzed a large, combined dataset from three distinct cohorts of comparably recruited patients with treatment-resistant depression who were treated with SCC-DBS. We assessed the critical role of WM recruitment in long-term therapeutic efficacy and thus the importance of precise connectome-based targeting for SCC-DBS. We employed voxel-level probabilistic stimulation mapping to retrospectively identify optimal stimulation zones for SCC-DBS. Based on individual stimulation modeling, we assessed the engagement of the predefined WM pathways used in tractography-based surgical planning, focusing on their contributions to sustained clinical improvements.

METHODS

Participants and Clinical Assessments

This study included 152 patients with treatment-resistant MDD for whom long-term follow-up data were available across three cohorts who received DBS implantation between 2003 and 2018 (12, 14, 18, 29, 34, 35, 39, 45–47). All participants provided written informed consent to participate in clinical trials. In cohort 1 (C1; University of Toronto; N=60) and cohort 2 (C2; BROADEN trial; N=55), anatomical landmark–based targeting was used. In cohort 3 (C3; Emory University; N=37) anatomical landmark– or connectome-based targeting was used. For C3 participants who underwent anatomical landmark–based targeting, DBS parameters were also adjusted using patient-specific connectivity data 6 months after the operation. C1 and C3 were from single-site studies; C2 was from a multisite industry-sponsored clinical trial. Data were shared in a de-identified manner. All protocols adhered to the Declaration of Helsinki and were approved by the institutional review boards at the respective institutions.

Across cohorts, patient selection criteria were similar but not identical. All studies required a diagnosis of MDD with a current episode lasting at least 2 years, a minimum score of 20 on the 17-item Hamilton Depression Rating Scale (HAM-D) (48), absence of psychiatric comorbidity, and failure of four different antidepressant treatments. In C2, although electroconvulsive therapy failure or intolerance was not a formal requirement, more than 80% of participants met this criterion (39).

All patients underwent bilateral SCC-DBS implantation using either Medtronic 3387 or St. Jude ActiveTip 6142-6145 electrodes targeting the SCC. Single surgeons implanted DBS electrodes in C1 and C3, and multiple surgeons performed implantations in C2. Inclusion criteria required 1) high-quality preoperative T1-weighted MRI and postoperative structural MRI or CT scans, 2) available DBS settings at 1- or 2-year postoperative time points, and 3) clinical symptom severity scores at both preoperative and postoperative stages corresponding to DBS settings. Depression severity was assessed using the HAM-D, which was consistently administered across all participants. Postoperative HAM-D scores were acquired at 2 years in C2 and C3, and at 1 year in C1, due to its limited 2-year follow-up. Clinical improvement was calculated as the percentage reduction in HAM-D scores from the preoperative baseline to the postoperative stage. A HAM-D score reduction threshold of ≥50% was used to define response. An exploratory linear regression analysis was performed before primary neuroimaging analyses to assess potential effects of covariates (age, sex, baseline severity, surgical targeting strategy, and electrode type) on clinical outcome. Since the surgical targeting strategy had inherent collinearity with the cohort and postoperative time point, these variables were not included in the regression analysis simultaneously.

Image Acquisition and Preprocessing

Preoperative T1-weighted structural MRI datasets were acquired (for C1, 1.5-T with complete brain coverage; for C2 and C3, 3-T with a 3-D magnetization-prepared rapid gradient-echo sequence). Postoperative structural MRI scans (for C1) and CT scans (for all three cohorts) were used for electrode localization. Postoperative scans were coregistered to preoperative T1-weighted images using Statistical Parametric Mapping (SPM12: https://www.fil.ion.ucl.ac.uk/spm/software/spm12; MRI to MRI) or Advanced Normalization Tools (ANTs: https://github.com/ANTsX/ANTs; CT to MRI). The coregistered images were normalized to the Montreal Neurological Institute (MNI) ICBM 2009b NLIN Asymmetric template space using ANTs (49, 50). Brain shift was corrected using a coarse mask (51). Bilateral DBS electrodes were localized in native space using TRAC/CORE and PaCER toolboxes (52, 53), and lead positions were transformed into template space using the warp fields from normalization. In the quality control process, 21 patients (12 from C1, seven from C2, two from C3) were excluded due to image noise that interfered with precise coregistration, normalization, or lead reconstruction. Bilateral volumes of tissue activated (VTAs) were

estimated in template space using individual postoperative DBS settings (active contact configuration and amplitude) via the FieldTrip-SimBio finite element method pipeline, applying a 0.2 V/mm threshold for electric field binarization (54, 55). All preprocessing was performed using the Lead-DBS toolbox (56), which incorporates these tools.

Voxel-Wise Comparison of Tissue Activation

Spatial (voxel-level) information of binary VTAs was retrospectively assessed to evaluate spatial stimulation patterns. Patients were divided into two groups: responders (HAM-D improvement ≥50%) and nonresponders. VTA center locations were analyzed to calculate spatial variance within and between groups. First, for within-group spatial variation, average distances between individuals within the group were calculated, and logistic regression was used with covariates of age, sex, cohort, and baseline severity. Additionally, linear regression (using clinical improvement as a continuous variable instead of a categorical responder/nonresponder variable) was used to test the robustness of findings. Second, for between-group spatial variance, the coordinates of VTA centers were compared between responders and nonresponders using Hotelling's t-squared test. Both analyses were conducted for each hemisphere, and Bonferroni correction was applied by adjusting p values for two comparisons corresponding to the two hemispheres. In an exploratory manner, both analyses were conducted for each cohort, with cohort excluded from the covariates.

Next, probabilistic stimulation mapping (PSM) was performed to identify anatomical regions where stimulation correlated with clinical improvement (57). As validated in prior work (58), the procedure involved 1) weighting individual VTAs by corresponding HAM-D improvements, 2) calculating voxel-wise t statistics to compare clinical improvements of subjects whose VTAs included a given voxel versus those whose VTAs did not, and 3) excluding voxels with <0.1 or >0.9 VTA overlap to reduce sample size imbalance in the t test. For an exploratory analysis, the distance between the peak PSM value and gray matter–white matter (GM-WM) boundary was calculated using a tissue probability map (59).

The PSM model's internal performance was evaluated using 10-fold and leave-one-cohort-out cross-validation (57, 58, 60). PSM was performed using only the VTAs of subjects in the training set. The t values (t statistics) of PSM voxels overlapping with the VTAs of each testing subject were summed to produce a VTA-PSM score. Importantly, the clinical improvements of testing subjects were not included in the calculation of their VTA-PSM scores. The VTA-PSM score quantifies the clinical importance of the spatial information of each VTA based on the training datasets. A linear association between VTA-PSM scores and clinical improvements was assessed using Pearson correlation and linear regression with covariates of age, sex, cohort, and baseline severity. Additionally, predictive performance on held-out data was quantified using Pearson's correlation coefficient (r); R^2, computed using the sum-of-squares formulation relative to a mean-only baseline; and root mean squared error (RMSE). Statistical significance for Pearson's correlation coefficients was assessed using 5,000-permutation tests. For contextual comparison, a mean-only (zeroR) baseline RMSE was computed within each training fold and evaluated on the held-out data. For 10-fold cross-validation, fold-wise r, R^2, and RMSE were summarized as means with standard deviations. For leave-one-cohort-out cross-validation, model performance was evaluated separately in each held-out cohort to assess cohort-specific generalization.

Fiber-Wise Analysis of White Matter Recruitment

Normative connectome data were used to assess the clinical role of WM fiber activation. This approach allows the analysis of SCC-DBS patients without individual diffusion MRI data, as normative streamlines (fibers) represent standardized WM structures shared across subjects (46). Normative WM fibers included in the left and right CBs, the FM, and the left and right medial uncinate fasciculus (mUF; also referred to as the ventral amygdala-fugal pathway) were selected using brain masks for surgical planning of connectome-based SCC-DBS (43, 61–63). The prior frontostriatal fiber is now considered together with the mUF in current surgical planning, where two different anatomical masks (seed and target) for each WM bundle capture the specific pathway. These mask pairs, which had been derived from individual tractography profiles of responders (34, 43), specified the CB with masks on the SCC and ventral anterior cingulate cortex, the FM with masks on the SCC and left and right ventromedial prefrontal cortices, and the mUF with masks on the SCC and diagonal band of Broca. Among all these fibers, those passing through individual VTAs were selected, representing activated fibers for each subject (64, 65).

Three methods were used to analyze WM activation. First, for common fiber activation, WM fibers activated in ≥90% of responders and nonresponders were identified separately to assess group differences. A conservative threshold of 100%, used in previous smaller-sample studies (29, 34, 35), rejected all fibers in this larger study, making it not feasible. After conducting iterative trials ranging from 80% to 100%, we selected 90% as a practical and conservative threshold that yielded reliable fiber activation.

Second, for fiber count comparison, the number of fibers from individual VTAs was compared between responders and nonresponders within each predefined WM bundle using logistic regression with covariates of age, sex, cohort, and baseline severity. Additionally, linear regression (with clinical improvement as a continuous outcome) was used to test the robustness of the findings. Bonferroni correction was applied by adjusting p values for five comparisons across the WM bundles. For exploratory analyses, the number of fibers was compared with clinical improvement within each cohort, and it was also compared between targeting strategies, using logistic and linear regression.

TABLE 1. Clinical characteristics of subcallosal cingulate deep brain stimulation across cohorts[a]

	Cohort 1 (N=48)		Cohort 2 (N=48)		Cohort 3 (N=35)	
Targeting strategy	Anatomical landmark		Anatomical landmark		Anatomical landmark, connectome	
	N	%	N	%	N	%
Female	30	62.50	28	58.33	21	60.00
Responders[b]	25	52.08	20	41.67	24	68.57
Nonresponders	23	47.92	28	58.33	11	31.43
	Mean	SD	Mean	SD	Mean	SD
Age (years)	46.25	8.15	47.25	11.27	46.45	9.93
Preoperative HAM-D score	25.85	3.14	20.79	4.18	23.00	2.42
Postoperative HAM-D score	12.75	7.62	12.13	7.52	8.31	5.18

[a] HAM-D, 17-item Hamilton Depression Rating Scale.
[b] Response was defined as reduction ≥50% in HAM-D score.

Third, for probabilistic fiber scoring, each WM fiber was scored based on its spatial overlap with PSM to quantify its contribution to clinical improvement. Specifically, the values of PSM voxels through which a given fiber passed were summed to produce a fiber-PSM score (fiber level). The distribution of fiber-PSM scores was visualized using histograms.

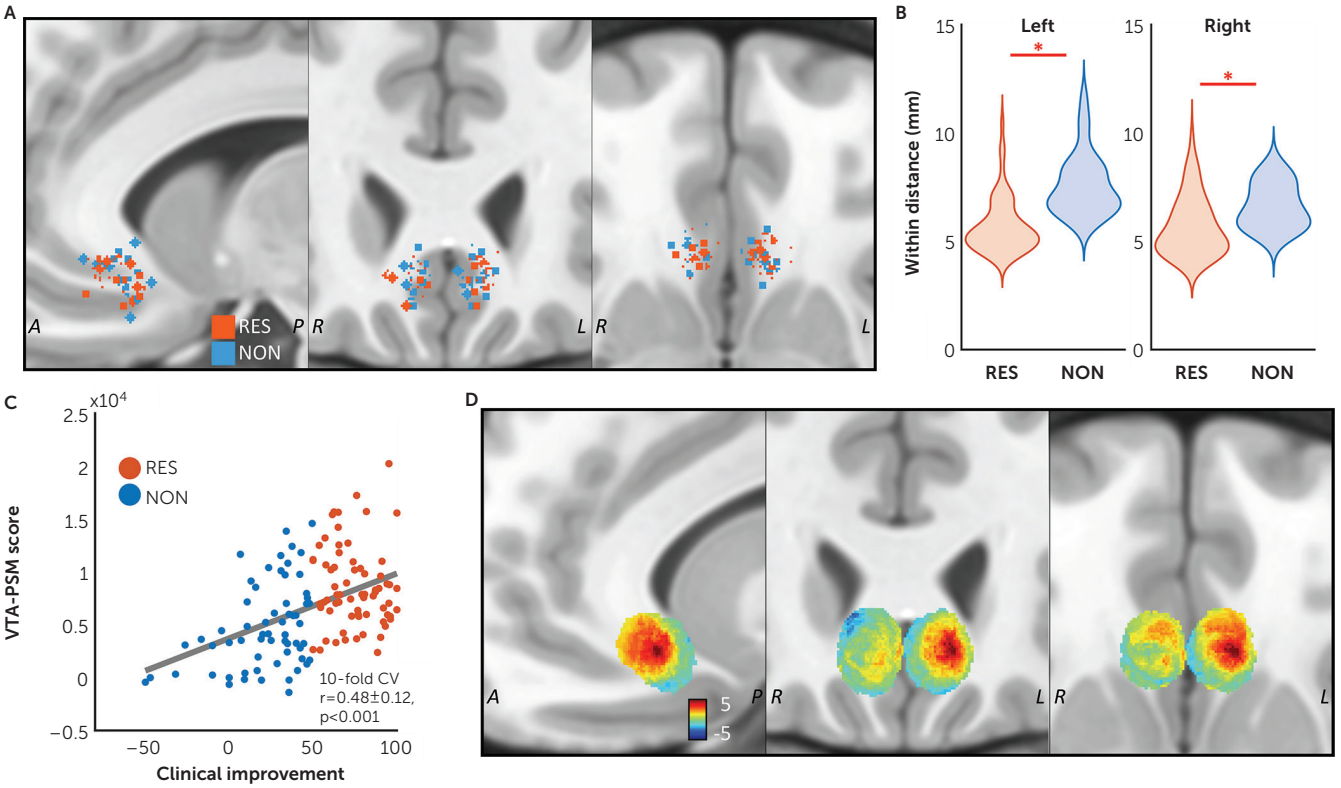
The fiber-PSM model's internal performance was evaluated using 10-fold and leave-one-cohort-out cross-validation. Again, PSM was performed using only the VTAs of subjects in the training set, and fiber-PSM scores were calculated for all fibers. Then, the fiber-PSM scores of activated fibers in each testing subject were summed to produce a summed fiber-PSM score (subject level). Importantly, the clinical improvements of testing subjects were not included in the calculation of their summed fiber-PSM scores. This score quantifies the clinical importance of activated fibers based on the training datasets. A linear association between summed fiber-PSM scores and clinical improvements was assessed using Pearson correlation and linear regression with covariates of age, sex, cohort, and baseline severity. Additionally, predictive performance on held-out data was quantified using r, R^2 computed using the sum-of-squares formulation relative to a mean-only baseline, and RMSE. The statistical significance of Pearson's correlation coefficients was assessed using 5,000-permutation tests. For contextual comparison, a mean-only (zeroR) baseline RMSE was computed within each training fold and evaluated on the held-out data. For 10-fold cross-validation, fold-wise r, R^2, and RMSE were summarized as means and standard deviations. For leave-one-cohort-out cross-validation, model performance was evaluated separately in each held-out cohort to assess cohort-specific generalization. In this procedure, different combinations of WM bundles were included in the model (left CB [CBL], right CB [CBR], FM, left mUF [mUFL], right mUF [mUFR], CBL+mUFL, CBR+mUFR, CBL+CBR+mUFL+mUFR, and CBL+CBR+FM+mUFL+mUFR), and Bonferroni correction was applied by adjusting p values for nine evaluations.

RESULTS

The analyses included 131 patients with treatment-resistant depression who underwent bilateral SCC-DBS (mean age=46.67 years, SD=9.79; 79 females). The patients exhibited an average improvement in HAM-D scores of 49.96% (SD=32.50) at 1- or 2-year postoperative time points, with 69 patients (52.67%) classified as responders (clinical improvement ≥50%) (Table 1; see also Table S1 in the online supplement). DBS targeting strategies varied by cohort, with anatomical landmark–based targeting used in C1 and C2, and either anatomical landmark–based (N=15) or connectome-based (N=20) targeting used in C3. An exploratory analysis using linear regression showed that surgical targeting strategy (0=anatomical landmark–based; 1=connectome-based) and baseline severity (preoperative HAM-D score) were significantly associated with clinical improvement (targeting strategy: β=20.93, 95% CI=4.67, 37.18; p=0.012; baseline severity: β=2.03, 95% CI=0.60, 3.46; p=0.006). Age, sex, and electrode type were not significantly associated with clinical improvement (age: β=−0.29, 95% CI=−0.85, 0.28; p=0.319; sex: β=4.52, 95% CI=−6.93, 15.97; p=0.436; electrode: β=−4.63, 95% CI=−24.51, 15.24; p=0.645).

A spatial (voxel-level) information analysis using logistic regression showed a significantly stronger within-group spatial concentration of target locations in responders compared to nonresponders after adjustment for age, sex, cohort, and baseline severity in both hemispheres (Figure 1A,B) (left: odds ratio=0.23, 95% CI=0.13, 0.39; corrected p<0.001; right: odds ratio=0.41, 95% CI=0.28, 0.61; corrected p<0.001). Additionally, linear regression showed consistent results (left: β=−11.09, 95% CI=−13.86, −8.33; corrected p<0.001; right: β=−8.82, 95% CI=−12.90, −4.75; corrected p<0.001). A cohort-specific analysis found a consistent pattern in the left hemisphere (see Figure S1 and Table S2 in the online supplement). When the coordinates of target locations were compared, no significant differences were observed between responders and nonresponders (left: T^2=3.31, df=3, 129, p=0.357; right: T^2=1.82, df=3, 129, p=0.618) (for cohort-specific results, see Table S3 in the online supplement).

FIGURE 1. Voxel-wise comparison of brain tissue activation[a]

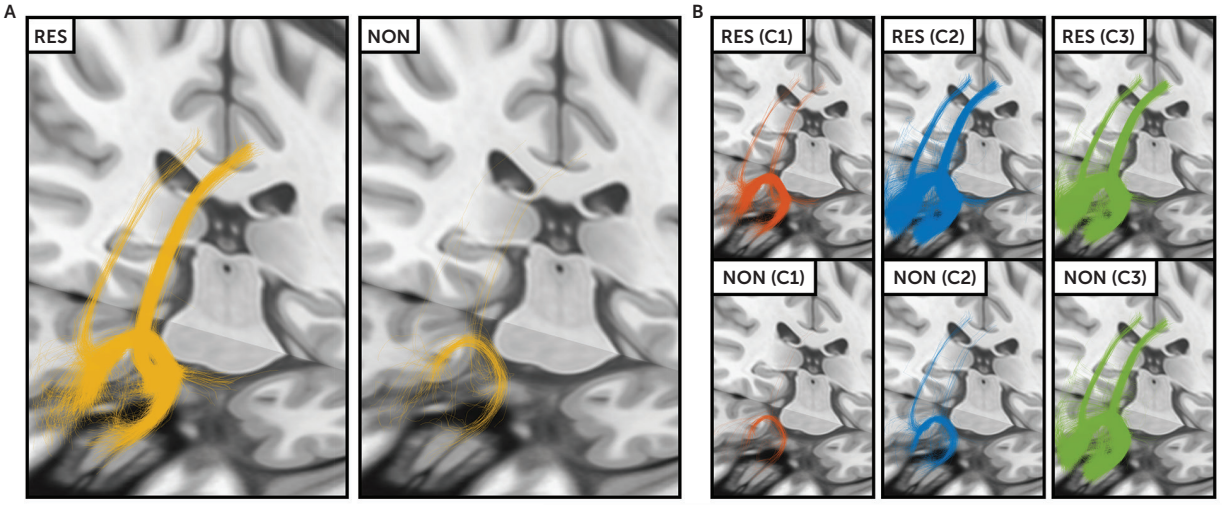


[a] Panel A shows the distribution of deep brain stimulation target (VTA center) locations for responders and nonresponders. Panel B shows within-group spatial distance of deep brain stimulation target locations in the left and right hemispheres. Responders exhibit stronger spatial clustering compared to nonresponders. Asterisks indicate significant differences between responders and nonresponders. Panel C shows a linear association between clinical improvement and VTA-PSM score estimated by a 10-fold out-of-sample procedure. Panel D shows PSM (t statistic map) in the left and right hemispheres. A, anterior; CV, cross-validation; L, left; NON, nonresponder; P, posterior; PSM, probabilistic stimulation mapping; R, right; RES, responder; VTA, volume of tissue activated.

In the left hemisphere, PSM covered 2,193 mm^3, with values ranging from 5.69 (peak voxel: x=−11.0, y=25.0, z=−9.0) to −2.39 (x=−1.0, y=26.5, z=−12.0). In the right hemisphere, PSM covered 2,151 mm^3, with values ranging from 3.15 (x=3.5, y=23.5, z=−9.5) to −3.77 (x=7.5, y=23.5, z=−2.0). Based on a tissue probability map, each PSM peak was located within 2 mm of the GM-WM boundary (left: 1.58 mm; right: 1.00 mm). The VTA-PSM score showed a significant linear association with clinical improvement (Figure 1C,D) (10-fold cross-validated Pearson's r=0.48, SD=0.12, p<0.001). This association remained statistically significant after adjustment for age, sex, cohort, and baseline severity (β=0.004, 95% CI=0.002, 0.005; p<0.001) (for cross-validated prediction performance metrics, see Figure S2A in the online supplement). When the VTA-PSM score in one cohort was generated from the other cohorts (leave-one-cohort-out), C1 and C2 showed a significant association with clinical improvement (see Figure S2B in the online supplement; C1: 10-fold cross-validation r=0.33, p=0.010; C2: 10-fold cross-validation r=0.49, p=0.001), whereas C3 did not (C3: 10-fold cross-validation r=0.20, p=0.121).

The common fiber activation analysis showed that fibers in the three hypothesized bundles (CB, FM, and mUF) were all activated in more than 90% of responders (Figure 2A) (number of fibers in CBL, 676; in CBR, 63; in FM, 24; in mUFL, 352; in mUFR, 35), whereas few or none of these were activated in nonresponders (number of fibers in CBL, 9; in CBR, 2; in FM, 0; in mUFL, 1; in mUFR, 3). Missing fibers in nonresponders were more pronounced in C1 and C2, with anatomical landmark–based targeting, compared to C3, where connectome-based targeting was used and group differences were less apparent (Figure 2B,C). Individual fiber count comparisons using logistic regression showed that responders had a greater number of activated fibers in the CBL and mUFL than nonresponders after adjustment for age, sex, cohort, and baseline severity (Figure 2D) (CBL: odds ratio=1.001, 95% CI=1.000, 1.002; corrected p<0.001; mUFL: odds ratio=1.010, 95% CI=1.005, 1.015; corrected p<0.001). Additional linear regression identified consistent results (CBL: β=0.02, 95% CI=0.01, 0.02; corrected p<0.001; mUFL: β=0.12, 95% CI=0.08, 0.15; corrected p<0.001). A cohort-specific analysis indicated that this pattern was underpowered in C3 specifically (see Figure S3 and Table S4 in the online supplement). An exploratory analysis found that connectome-based targeting resulted in a greater number of activated fibers compared

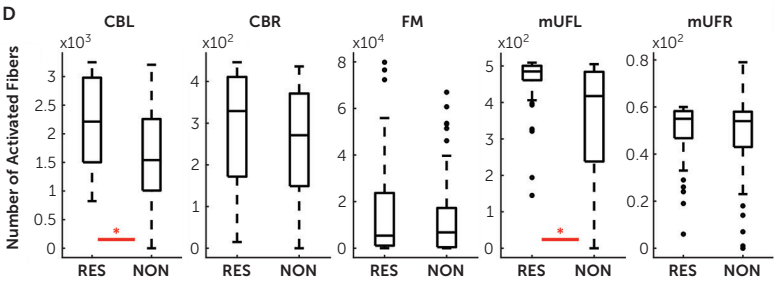
FIGURE 2. Common and individual white matter fiber activation analysis[a]



C

WM	All		C1		C2		C3	
	RES	NON	RES	NON	RES	NON	RES	NON
CBL	676	9	43	3	1207	15	1649	484
CBR	63	2	26	0	175	34	210	166
FM	24	0	11	4	733	12	1293	1694
mUFL	352	1	24	1	423	1	377	83
mUFR	35	3	29	0	43	20	33	31

Unit: number of WM fibers



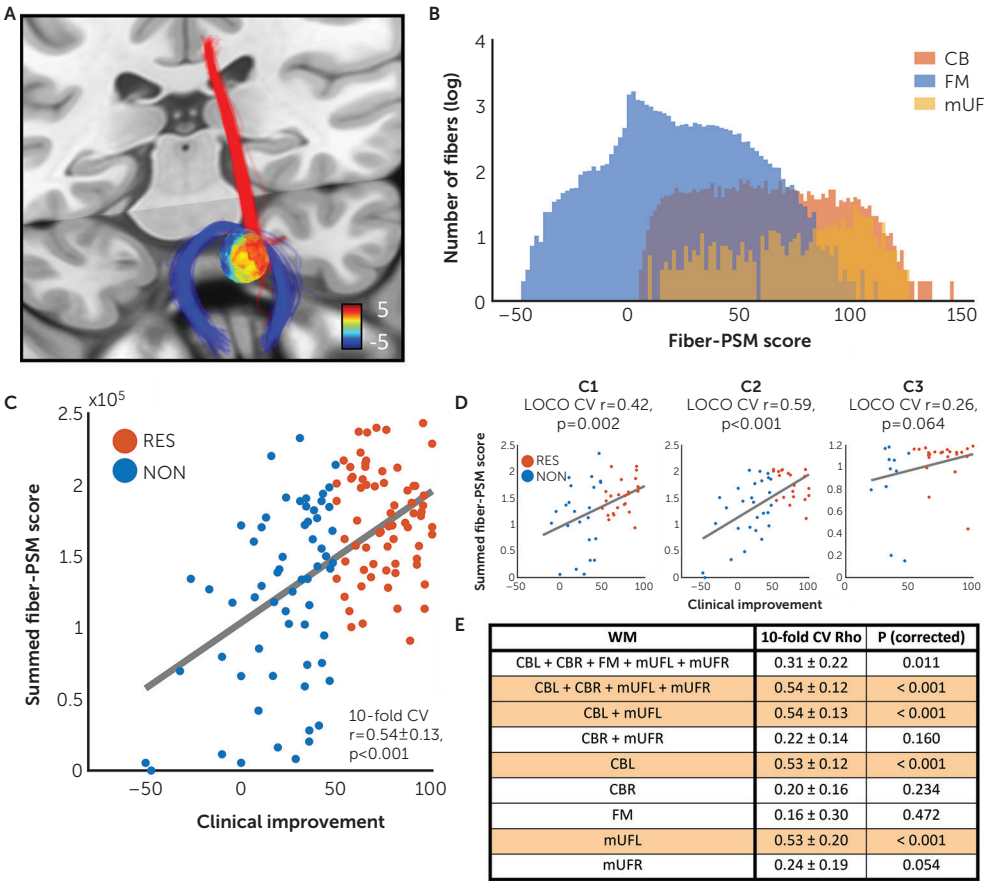
[a] Panel A shows common fibers activated (≥90%) in responders and nonresponders separately, and panel B shows common fiber activation within each cohort. Panel C shows counts of commonly activated fibers across responders and nonresponders shown in panels A and B. Panel D presents an individual fiber count comparison, showing that responders have a significantly greater number of activated fibers in the CBL and mUFL. Asterisks indicate significant differences between responders and nonresponders. C1–C3, cohorts 1–3; CBL, left cingulum bundle; CBR, right cingulum bundle; FM, forceps minor; mUFL, left medial uncinate fasciculus; mUFR, right medial uncinate fasciculus; NON, nonresponder; RES, responder; UFL, left uncinate fasciculus; UFR, right uncinate fasciculus; WM, white matter.

to anatomical landmark–based targeting (β=860.88, 95% CI=409.22, 1,312.55; p<0.001).

At the fiber level, the distribution of the fiber-PSM score showed that, although the FM had a greater number of activated fibers than the other bundles, the CB and mUF had activated fibers that contributed more to clinical improvement (Figure 3A,B) (fiber-PSM scores: CB=59.70, SD=1.02; FM=9.69, SD=0.17; mUF=78.32, SD=2.52). At the subject level, the summed fiber-PSM score showed a significant linear association with clinical improvement (Figure 3C) (10-fold cross-validated Pearson's r=0.54, SD=0.13, p<0.001). This association remained statistically significant after adjustment for age, sex, cohort, and baseline severity (β=0.0003, 95% CI=0.0002, 0.0004; p<0.001) (for cross-validated prediction performance metrics, see Figure S4A in the online supplement). When the summed fiber-PSM score in one cohort was generated from the other cohorts (leave-one-cohort-out), C1 and C2 showed a significant association with clinical improvement (Figure 3D; see also Figure S4B in the online supplement) (C1: 10-fold cross-validation r=0.42, p=0.002; C2: 10-fold cross-validation r=0.59, p<0.001), whereas C3 did not (C3: 10-fold cross-validation r=0.26, p=0.064). Across different combinations of WM bundles, models including the left CB and/or mUF showed statistically significant cross-validated correlations (Figure 3E).

For held-out prediction performance in 10-fold cross-validation, cross-validated correlations between empirical and predicted clinical improvement derived from both VTA-PSM and fiber-PSM models were statistically significant (see Figures S2A and S4A in the online supplement). Models based on the VTA-PSM score, together with covariates (age, sex, cohort, and baseline severity), yielded positive out-of-sample R^2 values and lower RMSE compared with a mean-only (zeroR) baseline (12% reduction in RMSE; see Figure S2A in the online supplement). Models based on the summed fiber-PSM score also yielded positive out-of-sample R^2 values and lower RMSE relative to the mean-only baseline (16% reduction; see Figure S4A and Table S5 in the online supplement). In leave-one-cohort-out cross-validation, significant cross-validated correlations between empirical and predicted clinical improvement were observed in held-out cohorts C1 and C2 but not in C3 (see Figures S2B and S4B in the online supplement). Across analyses, inclusion of

FIGURE 3. Activated white matter fiber quantification based on probabilistic stimulation mapping[a]



WM	10-fold CV Rho	P (corrected)
CBL + CBR + FM + mUFL + mUFR	0.31 ± 0.22	0.011
CBL + CBR + mUFL + mUFR	0.54 ± 0.12	< 0.001
CBL + mUFL	0.54 ± 0.13	< 0.001
CBR + mUFR	0.22 ± 0.14	0.160
CBL	0.53 ± 0.12	< 0.001
CBR	0.20 ± 0.16	0.234
FM	0.16 ± 0.30	0.472
mUFL	0.53 ± 0.20	< 0.001
mUFR	0.24 ± 0.19	0.054

[a] Panel A shows examples of activated fibers based on the fiber-PSM score (fiber level), with the 100 highest-scoring (red) and 100 lowest-scoring (blue) fibers visualized. Panel B is a histogram of fiber-PSM scores for all fibers included in critical WM bundles. Panels C and D show linear associations between clinical improvement and summed fiber-PSM score (subject level), estimated by 10-fold and LOCO out-of-sample procedures, respectively. Panel E reports the linear association between clinical improvement and summed fiber-PSM score across different combinations of WM bundles in 10-fold out-of-sample procedures. C1–C3, cohorts 1–3; CB, cingulum bundle; CBL, left CB; CBR, right CB; CV, cross-validation; FM, forceps minor; LOCO, leave-one-cohort-out; mUFL, left medial UF; mUFR, right medial UF; NON, nonresponder; PSM, probabilistic stimulation mapping; RES, responder; UF, uncinate fasciculus; WM, white matter.

covariates (age, sex, and baseline severity) did not materially alter cross-validated correlation patterns.

DISCUSSION

Using a combined dataset from three cohorts of patients with treatment-resistant depression who were treated with SCC-DBS, we investigated connectomic factors associated with long-term clinical improvement. These voxel- and fiber-level analyses suggest that stimulation of specific locations, particularly in the left hemisphere, was linked to sustained HAM-D score reductions at 1- or 2-year follow-up. Our findings further suggest that the absence of activation in the left CB or uncinate fasciculus may reduce the clinical benefits of SCC-DBS.

Connectomic Factors Underlying SCC-DBS

This study examined the distribution of 131 target locations in each hemisphere and found that the spatial concentration of VTAs in responders formed a focal cluster on PSM, without a significant difference in the central anatomical coordinates between responders and nonresponders. This cluster, located within 2 mm of the GM-WM boundary, suggests that deviations toward either GM or WM may limit therapeutic effects, indicating the importance of balancing potential DBS effects across both tissue types. This implies that both the initial rationale for SCC-DBS, namely, controlling hyperactivity of GM, and more recent evidence emphasizing the necessity of WM modulation of the connected regions and associated networks may converge for ideal clinical outcomes (6, 10, 29, 43).

This spatial cluster on PSM was spatially aligned with commonly activated fibers. Previous studies have suggested the importance of recruiting WM bundles in SCC-DBS outcomes and proposed a prospective tractography-based targeting strategy (29, 34, 35). This targeting strategy has evolved, and our study focused on specific WM pathways (CB, FM, and mUF) that are routinely targeted by our group for current surgical planning of patient-specific connectome-based SCC-DBS (34, 43), in contrast to other studies that used normative connectome data to identify clinically relevant WM tracts retrospectively (66). Our observation of qualitative differences in commonly activated fibers between responders and nonresponders supports the potential relevance of engaging specific WM pathways for optimal clinical efficacy (29).

In the fiber count and scoring analyses, statistical significance was observed for the left CB and mUF. Bilateral DBS has been the standard approach for achieving stable and sustained clinical response, yet previous studies have noted a stronger contribution of left-sided DBS to both acute behavioral and physiological effects (29, 35, 42, 44, 67–69) as well as overall clinical improvement (35, 66, 70). However, no studies demonstrate that response can be reliably achieved with left-sided DBS alone (70), and a single case shows the opposite to be true (71). Further, in more recent electrophysiological

studies, there are independent contributions of both right and left hemisphere stimulation, and a delay in one over the other is associated with delayed response times and nonresponse (43).

Cohort-Level Variability and Connectome-Based Targeting

The importance of WM activation for SCC-DBS has become increasingly recognized. Individual diffusion MRI data were available for the more recent cohort (C3) (6, 34, 35) but not the others, which limited direct comparisons. In this study, the use of normative connectome data allowed comparable within- and between-cohort analyses.

Although the BROADEN industry-sponsored randomized controlled trial (C2) relied on anatomical landmark–based targeting without diffusion MRI and did not demonstrate clinical efficacy 6 months after surgery (39), approximately 50% of participants who continued treatment achieved a response by 18 months (18). Our findings suggest that those who showed no response despite ongoing DBS and adjustments may have had insufficient activation of critical WM bundles. These results support the importance of tractography-based precision targeting and DBS parameter programming to maximize connectome-based target engagement.

In PSM-based analyses (both VTA-PSM and fiber-PSM) using a leave-one-cohort-out approach, linear associations with clinical improvement identified in the remaining cohorts generalized to held-out cohorts C1 and C2. In contrast, these associations did not generalize to C3, a cohort in which connectome-based targeting was applied. Exploratory analysis suggested that connectome-based targeting increased the overall number of activated fibers, which may have resulted in less distinct connectomic patterns across clinical improvements in C3 compared with the other cohorts. While this likely reflects improved consistency of surgical targeting, it also limits discrimination across clinical outcomes when normative connectome data are used. These findings suggest that WM engagement may be necessary but not sufficient for antidepressant response. However, considering the macroscale WM estimation in this study and the potentially limited sensitivity of normative connectome data, further work is warranted, such as analyzing WM subdivisions, and/or using patient-specific diffusion MRI datasets that incorporate WM integrity measures (43).

Individual Variability and Limitations

Normative connectome data have been proposed as a way to facilitate wider access to DBS for neuropsychiatric disorders (46, 65, 72, 73). Indeed, the use of normative connectome data for retrospective analyses offers high-quality WM information (56, 65, 74–76), may reduce false positives, and allows for fiber-level analyses without requiring individual diffusion MRI data analyses, which are not part of routine clinical DBS implantation procedures (77–80). However, normative data cannot capture individual variability, such as differences in structural connectivity or WM abnormalities, which may affect SCC-DBS outcomes (43, 81, 82). Moreover, normative connectome data are inherently constrained by anatomical standardization: Without individual variability in connectivity profiles, a putative ideal target derived from normative connectome data would appear uniformly identical across subjects.

These limitations may partially explain deviations from prior studies that used patient-specific diffusion MRI data (29, 34, 35, 44). In our study, right-sided bundles and the FM did not reach statistical significance, suggesting that their contribution may be less consistent across methodologies and warranting further exploration using individual diffusion MRI data (43). In particular, when connectome-based targeting and stimulation parameter adjustment were applied in C3, normative streamlines alone were not sufficient to fully identify the source of nonresponse. Even though VTAs in responders did not converge on a single anatomical location, they may have shared common structural connectivity patterns, such as consistently high activation of the CB, which normative data alone may not capture. This was suggested by previous studies where small differences in target location produced distinctive effects on patient-specific tractography and stimulation-induced physiological responses, highlighting the necessity of patient-specific neuroimaging measures and their reproducibility (41, 83–85).

In addition, advanced cable and electric field models using individual diffusion MRI data would allow more accurate and detailed estimation of WM engagement by SCC-DBS, incorporating patient-specific WM integrity and electrode/axon orientation (41, 44, 83, 86). A prior study using these approaches (44) reported differences in estimated WM engagement compared with normative connectome-based analyses, highlighting the clinical relevance of the CB and FM rather than the uncinate fasciculus. Together, these findings motivate further validation of the present results using accurate, patient-specific WM modeling.

While this study integrated SCC-DBS data from three cohorts to identify common connectomic factors associated with long-term clinical improvement, there was limited availability of 2-year follow-up data in C1, so the 1-year time point data were used, which may introduce minor variability. However, the 1-year data still provide meaningful insight into longer-term clinical trajectories. Additionally, while our analyses adjusted for the cohort-specific factor, it was not possible to fully disentangle the effects of cohorts, targeting strategies, and time points, because of their inherent collinearity. Supplementary analyses restricted to single-site cohorts examined potential temporal or surgery-sequence effects and did not suggest a strong influence of implantation sequence on observed outcomes (see Figure S5 in the online supplement). Furthermore, a single DBS setting may not represent the patient's long-term stimulation settings. In most cases, changes in contact placement and in dose of current administered are typically made in the first year to improve outcomes in nonresponders or to recapture response in unstable responders.

In general, once a stable response is achieved, it is maintained long-term.

There are also factors beyond surgical targeting that contribute to DBS nonresponse, most notably patient-specific clinical characteristics that might favor an alternative DBS target (5, 87), as well as potentially other sources of clinical variability, including masked comorbidity at the time of enrollment, such as anxiety, inflammation (43, 88, 89), or other sources of variance in network dysfunction (90). In addition, cohort-specific contextual and psychosocial factors, such as differences in referral pathways, motivation, and social support, may further influence outcomes and differ meaningfully across study designs. While beyond the scope of this study or DBS work to date, as with other treatments, matching patients to their brain type rather than symptom profile holds great promise (91, 92). Together, these considerations highlight the multifactorial nature of therapeutic response to SCC-DBS and underscore the need for measured interpretation of the results. Further studies will be needed to evaluate these influences as this surgical treatment is refined, optimized, and scaled for clinical use (27, 43, 93–95).

Despite these limitations, we anticipate that our hypothesis-driven approach, or one like it focusing on consistent targeting of these three WM bundles, can help guide the design of clinical trials of SCC-DBS. In addition to demonstrating robust clinical outcomes, a systematic targeting strategy based on patient-specific connectomic factors may be an important consideration for regulatory approval and broader clinical implementation of SCC-DBS. However, simplification of the multistep diffusion MRI data analysis procedure will be needed for its adoption and routine use.

Over the past two decades of SCC-DBS, targeting refinement for treatment-resistant depression has continued to evolve, sustained by patients who have achieved long-term recovery with ongoing stimulation (12, 14). Scalable methods to improve accuracy and precision may be further enhanced by applying connectome-based targeting, which prioritizes circuits over anatomical landmarks and aims to ensure necessary WM pathway activation in each subject. This study of both early and recent SCC-DBS cohorts uniquely investigated sustained clinical improvement with ongoing chronic DBS treatment and provides evidence supporting the efficacy of connectome-based targeting.

AUTHOR AND ARTICLE INFORMATION

[1]Nash Family Center for Advanced Circuit Therapeutics, Icahn School of Medicine at Mount Sinai, New York. [2]Center for Neuromodulation, Icahn School of Medicine at Mount Sinai, New York. [3]Department of Psychiatry and Behavioral Sciences, Emory University School of Medicine, Atlanta. [4]Joint Department of Medical Imaging, University of Toronto, Toronto. [5]Krembil Brain Institute, Toronto Western Hospital, University Health Network, Toronto. [6]Institute of Biomedical Engineering, University of Toronto, Toronto. [7]Department of Psychiatry, University of Toronto, Toronto. [8]Abbott Neuromodulation, Plano, TX. [9]Department of Neurosurgery, Rutgers Robert Wood Johnson Medical School, New Brunswick, NJ. [10]Division of Neurosurgery, Department of Surgery, University Health Network, Toronto.

Send correspondence to Dr. Choi (kisueng.choi@mssm.edu).

Mr. Song https://orcid.org/0000-0002-8915-0763

Dr. Figee https://orcid.org/0000-0003-3679-284X

Dr. Germann https://orcid.org/0000-0003-0995-8226

This work was supported by the NIH BRAIN Initiative through NINDS grant UH3NS103550, the Hope for Depression Research Foundation, and the DANA Foundation. Devices were donated by St. Jude Medical (now Abbott) and Medtronic.

Dr. Choi has served as a consultant for Abbott. Dr. Kopell has served as a consultant for Abbott, Medtronic, and Turing. Dr. Figee has served as a consultant for Abbott and Medtronic. Dr. Riva-Posse has served as a consultant for Abbott, Janssen Pharmaceuticals, LivaNova, Medtronic, and Motif. Dr. Elias has intellectual property in the field of DBS. Drs. Himes and Cheeran are employees of Abbott, a DBS device manufacturer and sponsor of the BROADEN and TRANSCEND studies. Dr. Lozano has served as a consultant for Abbott, Boston Scientific, Functional Neuromodulation (Scientific Director), Insightec, and Medtronic. Dr. Mayberg has served as a consultant for Abbott Neuromodulation, AbbVie, BlackrockNeuro, and NextSense; she receives intellectual property licensing fees from Abbott Neuromodulation; and she has served on scientific advisory boards for the Brain and Behavior Research Foundation and the Klingenstein Foundation. The other authors report no financial relationships with commercial interests.

Received May 2, 2025; final revision received February 25, 2026; accepted May 18, 2026.

REFERENCES

1. Bromet E, Andrade LH, Hwang I, et al: Cross-national epidemiology of DSM-IV major depressive episode. BMC Med 2011; 9:90
2. Gelenberg AJ: A review of the current guidelines for depression treatment. J Clin Psychiatry 2010; 71:e15
3. Fogelson DL, Leuchter A: Defining treatment-resistant depression. JAMA Psychiatry 2017; 74:758–759
4. Gaynes BN, Lux L, Gartlehner G, et al: Defining treatment-resistant depression. Depress Anxiety 2020; 37:134–145
5. Johnson KA, Okun MS, Scangos KW, et al: Deep brain stimulation for refractory major depressive disorder: a comprehensive review. Mol Psychiatry 2024; 29:1075–1087
6. Choi KS, Mayberg H: Connectomic DBS in major depression; in Connectomic Deep Brain Stimulation. Edited by Horn A. London, Academic Press, 2022, pp 433–447
7. Kleiner-Fisman G, Herzog J, Fisman DN, et al: Subthalamic nucleus deep brain stimulation: summary and meta-analysis of outcomes. Mov Disord 2006; 21(Suppl 14):S290–S304
8. Litvak V, Jha A, Eusebio A, et al: Resting oscillatory cortico-subthalamic connectivity in patients with Parkinson's disease. Brain 2011; 134:359–374
9. Holtzheimer PE, Mayberg HS: Deep brain stimulation for psychiatric disorders. Annu Rev Neurosci 2011; 34:289–307
10. Mayberg HS, Lozano AM, Voon V, et al: Deep brain stimulation for treatment-resistant depression. Neuron 2005; 45:651–660
11. Mayberg HS: Targeted electrode-based modulation of neural circuits for depression. J Clin Invest 2009; 119:717–725
12. Kennedy SH, Giacobbe P, Rizvi SJ, et al: Deep brain stimulation for treatment-resistant depression: follow-up after 3 to 6 years. Am J Psychiatry 2011; 168:502–510
13. Kisely S, Li A, Warren N, et al: A systematic review and meta-analysis of deep brain stimulation for depression. Depress Anxiety 2018; 35:468–480
14. Crowell AL, Riva-Posse P, Holtzheimer PE, et al: Long-term outcomes of subcallosal cingulate deep brain stimulation for treatment-resistant depression. Am J Psychiatry 2019; 176:949–956
15. Clark DL, Johnson KA, Butson CR, et al: Tract-based analysis of target engagement by subcallosal cingulate deep brain stimulation for treatment resistant depression. Brain Stimul 2020; 13:1094–1101

16. Brown EC, Clark DL, Forkert ND, et al: Metabolic activity in subcallosal cingulate predicts response to deep brain stimulation for depression. Neuropsychopharmacology 2020; 45:1681–1688
17. Martínez GV, Justicia A, Salgado P, et al: A randomized trial of deep brain stimulation to the subcallosal cingulate and nucleus accumbens in patients with treatment-refractory, chronic, and severe anorexia nervosa: initial results at 6 months of follow up. J Clin Med 2020; 9:1946
18. Himes LM, Mayberg HS, Husain MM, et al: Revisiting subcallosal cingulate deep brain stimulation for depression: long-term safety and effectiveness outcomes from a pooled analysis of 172 implanted patients. Brain Stimul 2025; 18:1632–1640
19. Williams LM: Precision psychiatry: a neural circuit taxonomy for depression and anxiety. Lancet Psychiatry 2016; 3:472–480
20. Mayberg HS: Limbic-cortical dysregulation: a proposed model of depression. J Neuropsychiatry Clin Neurosci 1997; 9:471–481
21. Li B-J, Friston K, Mody M, et al: A brain network model for depression: from symptom understanding to disease intervention. CNS Neurosci Ther 2018; 24:1004–1019
22. Greicius MD, Flores BH, Menon V, et al: Resting-state functional connectivity in major depression: abnormally increased contributions from subgenual cingulate cortex and thalamus. Biol Psychiatry 2007; 62:429–437
23. Menon V: 20 years of the default mode network: a review and synthesis. Neuron 2023; 111:2469–2487
24. Mayberg HS, Liotti M, Brannan SK, et al: Reciprocal limbic-cortical function and negative mood: converging PET findings in depression and normal sadness. Am J Psychiatry 1999; 156:675–682
25. Mayberg HS, Brannan SK, Tekell JL, et al: Regional metabolic effects of fluoxetine in major depression: serial changes and relationship to clinical response. Biol Psychiatry 2000; 48:830–843
26. Yeo BTT, Krienen FM, Sepulcre J, et al: The organization of the human cerebral cortex estimated by intrinsic functional connectivity. J Neurophysiol 2011; 106:1125–1165
27. Dunlop BW, Cha J, Choi KS, et al: Shared and unique changes in brain connectivity among depressed patients after remission with pharmacotherapy versus psychotherapy. Am J Psychiatry 2023; 180:218–229
28. Merkl A, Neumann W-J, Huebl J, et al: Modulation of beta-band activity in the subgenual anterior cingulate cortex during emotional empathy in treatment-resistant depression. Cereb Cortex 2016; 26:2626–2638
29. Riva-Posse P, Choi KS, Holtzheimer PE, et al: Defining critical white matter pathways mediating successful subcallosal cingulate deep brain stimulation for treatment-resistant depression. Biol Psychiatry 2014; 76:963–969
30. Gutman DA, Holtzheimer PE, Behrens TEJ, et al: A tractography analysis of two deep brain stimulation white matter targets for depression. Biol Psychiatry 2009; 65:276–282
31. Johansen-Berg H, Gutman DA, Behrens TEJ, et al: Anatomical connectivity of the subgenual cingulate region targeted with deep brain stimulation for treatment-resistant depression. Cereb Cortex 2008; 18:1374–1383
32. Dosenbach NUF, Raichle ME, Gordon EM: The brain's action-mode network. Nat Rev Neurosci 2025; 26:158–168
33. Gordon EM, Chauvin RJ, Van AN, et al: A somato-cognitive action network alternates with effector regions in motor cortex. Nature 2023; 617:351–359
34. Riva-Posse P, Choi KS, Holtzheimer PE, et al: A connectomic approach for subcallosal cingulate deep brain stimulation surgery: prospective targeting in treatment-resistant depression. Mol Psychiatry 2018; 23:843–849
35. Choi KS, Riva-Posse P, Gross RE, et al: Mapping the "depression switch" during intraoperative testing of subcallosal cingulate deep brain stimulation. JAMA Neurol 2015; 72:1252–1260
36. Heilbronner SR, Haber SN: Frontal cortical and subcortical projections provide a basis for segmenting the cingulum bundle: implications for neuroimaging and psychiatric disorders. J Neurosci 2014; 34:10041–10054
37. Petrides M, Pandya DN: Efferent association pathways from the rostral prefrontal cortex in the macaque monkey. J Neurosci 2007; 27:11573–11586
38. Barbas H, Zikopoulos B: Toward patient-specific targeting and parameter setting of deep brain stimulation for relief of depression. Biol Psychiatry 2014; 76:914–916
39. Holtzheimer PE, Husain MM, Lisanby SH, et al: Subcallosal cingulate deep brain stimulation for treatment-resistant depression: a multisite, randomised, sham-controlled trial. Lancet Psychiatry 2017; 4:839–849
40. Noecker AM, Choi KS, Riva-Posse P, et al: StimVision software: examples and applications in subcallosal cingulate deep brain stimulation for depression. Neuromodulation 2018; 21:191–196
41. Lujan JL, Chaturvedi A, Choi KS, et al: Tractography-activation models applied to subcallosal cingulate deep brain stimulation. Brain Stimul 2013; 6:737–739
42. Riva-Posse P, Crowell AL, Wright K, et al: Rapid antidepressant effects of deep brain stimulation and their relation to surgical protocol. Biol Psychiatry 2020; 88:e37–e39
43. Alagapan S, Choi KS, Heisig S, et al: Cingulate dynamics track depression recovery with deep brain stimulation. Nature 2023; 622:130–138
44. Howell B, Choi KS, Gunalan K, et al: Quantifying the axonal pathways directly stimulated in therapeutic subcallosal cingulate deep brain stimulation. Hum Brain Mapp 2019; 40:889–903
45. Lozano AM, Mayberg HS, Giacobbe P, et al: Subcallosal cingulate gyrus deep brain stimulation for treatment-resistant depression. Biol Psychiatry 2008; 64:461–467
46. Elias GJB, Germann J, Joel SE, et al: A large normative connectome for exploring the tractographic correlates of focal brain interventions. Sci Data 2024; 11:353
47. Lozano AM, Giacobbe P, Hamani C, et al: A multicenter pilot study of subcallosal cingulate area deep brain stimulation for treatment-resistant depression. J Neurosurg 2012; 116:315–322
48. Hamilton M: A rating scale for depression. J Neurol Neurosurg Psychiatry 1960; 23:56–62
49. Fonov V, Evans AC, Botteron K, et al: Unbiased average age-appropriate atlases for pediatric studies. Neuroimage 2011; 54:313–327
50. Ewert S, Horn A, Finkel F, et al: Optimization and comparative evaluation of nonlinear deformation algorithms for atlas-based segmentation of DBS target nuclei. Neuroimage 2019; 184:586–598
51. Avants BB, Tustison NJ, Song G, et al: A reproducible evaluation of ANTs similarity metric performance in brain image registration. Neuroimage 2011; 54:2033–2044
52. Horn A, Kuhn AA: Lead-DBS: a toolbox for deep brain stimulation electrode localizations and visualizations. Neuroimage 2015; 107:127–135
53. Husch A, Petersen MV, Gemmar P, et al: PaCER: a fully automated method for electrode trajectory and contact reconstruction in deep brain stimulation. Neuroimage Clin 2017; 17:80–89
54. Vorwerk J, Oostenveld R, Piastra MC, et al: The FieldTrip-SimBio pipeline for EEG forward solutions. Biomed Eng Online 2018; 17:37
55. Astrom M, Diczfalusy E, Martens H, et al: Relationship between neural activation and electric field distribution during deep brain stimulation. IEEE Trans Biomed Eng 2015; 62:664–672
56. Horn A, Li N, Dembek TA, et al: Lead-DBS v2: towards a comprehensive pipeline for deep brain stimulation imaging. Neuroimage 2019; 184:293–316
57. Elias GJB, Boutet A, Joel SE, et al: Probabilistic mapping of deep brain stimulation: insights from 15 years of therapy. Ann Neurol 2021; 89:426–443
58. Reich MM, Horn A, Lange F, et al: Probabilistic mapping of the antidystonic effect of pallidal neurostimulation: a multicentre imaging study. Brain 2019; 142:1386–1398
59. Ashburner J, Friston KJ: Unified segmentation. Neuroimage 2005; 26:839–851

60. Ríos AS, Oxenford S, Neudorfer C, et al: Optimal deep brain stimulation sites and networks for stimulation of the fornix in Alzheimer's disease. Nat Commun 2022; 13:7707
61. Avecillas-Chasin JM, Justo M, Levinson S, et al: Structural correlates of emotional response to electrical stimulation of the amygdala in subjects with PTSD. Brain Stimul 2020; 13:424–426
62. Kamali A, Sair HI, Blitz AM, et al: Revealing the ventral amygdalofugal pathway of the human limbic system using high spatial resolution diffusion tensor tractography. Brain Struct Funct 2016; 221:3561–3569
63. Bullock DN, Hayday EA, Grier MD, et al: A taxonomy of the brain's white matter: twenty-one major tracts for the 21st century. Cereb Cortex 2022; 32:4524–4548
64. Butenko K, Van Rienen U: DBS imaging methods III: estimating the electric field and volume of tissue activated; in Connectomic Deep Brain Stimulation. Edited by Horn A. London, Academic Press, 2022, pp 147–168
65. Elias GJB, Germann J, Loh A, et al: Normative connectomes and their use in DBS; in Connectomic Deep Brain Stimulation. Edited by Horn A. London, Academic Press, 2022, pp 245–274
66. Elias GJB, Germann J, Boutet A, et al: Local neuroanatomical and tract-based proxies of optimal subcallosal cingulate deep brain stimulation. Brain Stimul 2023; 16:1259–1272
67. Sendi MSE, Waters AC, Tiruvadi V, et al: Intraoperative neural signals predict rapid antidepressant effects of deep brain stimulation. Transl Psychiatry 2021; 11:551
68. Riva-Posse P, Inman CS, Choi KS, et al: Autonomic arousal elicited by subcallosal cingulate stimulation is explained by white matter connectivity. Brain Stimul 2019; 12:743–751
69. Smart O, Choi KS, Riva-Posse P, et al: Initial unilateral exposure to deep brain stimulation in treatment-resistant depression patients alters spectral power in the subcallosal cingulate. Front Comput Neurosci 2018; 12:43
70. Conroy SK, Malloy S, Kelley ME, et al: Left versus right subcallosal cingulate deep brain stimulation for treatment-resistant depression. Pers Med Psychiatry 2021; 25–26:100069
71. Guinjoan SM, Mayberg HS, Costanzo EY, et al: Asymmetrical contribution of brain structures to treatment-resistant depression as illustrated by effects of right subgenual cingulum stimulation. J Neuropsychiatry Clin Neurosci 2010; 22:265–277
72. Horn A, Reich M, Vorwerk J, et al: Connectivity predicts deep brain stimulation outcome in Parkinson disease. Ann Neurol 2017; 82:67–78
73. Hollunder B, Rajamani N, Siddiqi SH, et al: Toward personalized medicine in connectomic deep brain stimulation. Prog Neurobiol 2022; 210:102211
74. Glasser MF, Sotiropoulos SN, Wilson JA, et al: The minimal preprocessing pipelines for the Human Connectome Project. Neuroimage 2013; 80:105–124
75. Setsompop K, Kimmlingen R, Eberlein E, et al: Pushing the limits of in vivo diffusion MRI for the Human Connectome Project. Neuroimage 2013; 80:220–233
76. Horn A (ed): Connectomic Deep Brain Stimulation. London, Academic Press, 2022
77. Horn A, Blankenburg F: Toward a standardized structural-functional group connectome in MNI space. Neuroimage 2016; 124:310–322
78. Fox MD: Mapping symptoms to brain networks with the human connectome. N Engl J Med 2018; 379:2237–2245
79. Chang B, Park JJ, Buch VP: Applying normative atlases in deep brain stimulation: a comprehensive review. Int J Surg 2024; 110:8037–8044
80. Neudorfer C, Butenko K, Oxenford S, et al: Lead-DBS v3.0: mapping deep brain stimulation effects to local anatomy and global networks. Neuroimage 2023; 268:119862
81. Wang Q, Akram H, Muthuraman M, et al: Normative vs patient-specific brain connectivity in deep brain stimulation. Neuroimage 2021; 224:117307
82. Coenen VA, Schlaepfer TE, Varkuti B, et al: Surgical decision making for deep brain stimulation should not be based on aggregated normative data mining. Brain Stimul 2019; 12:1345–1348
83. Seas A, Noor MS, Choi KS, et al: Subcallosal cingulate deep brain stimulation evokes two distinct cortical responses via differential white matter activation. Proc Natl Acad Sci U S A 2024; 121:e2314918121
84. Song HN, Kopell BH, Mayberg HS, et al: Variability of individual white matter connectivity in subcallosal cingulate deep brain stimulation target for treatment-resistant depression; poster presented at the 2024 NYC Neuromodulation conference, New York, August 1–3, 2024
85. Waters AC, Veerakumar A, Choi KS, et al: Test-retest reliability of a stimulation-locked evoked response to deep brain stimulation in subcallosal cingulate for treatment resistant depression. Hum Brain Mapp 2018; 39:4844–4856
86. Howell B, McIntyre CC: Analyzing the tradeoff between electrical complexity and accuracy in patient-specific computational models of deep brain stimulation. J Neural Eng 2016; 13:036023
87. Scangos KW, Khambhati AN, Daly PM, et al: Closed-loop neuromodulation in an individual with treatment-resistant depression. Nat Med 2021; 27:1696–1700
88. Cha J, Raj D, Choi KS, et al: Impact of inflammation on white matter integrity and functional connectivity in chronic major depressive disorder. Biol Psychiatry 2025; 99:660–670
89. Dougherty DD, Weiss AP, Cosgrove GR, et al: Cerebral metabolic correlates as potential predictors of response to anterior cingulotomy for treatment of major depression. J Neurosurg 2003; 99:1010–1017
90. Drysdale AT, Grosenick L, Downar J, et al: Resting-state connectivity biomarkers define neurophysiological subtypes of depression. Nat Med 2017; 23:28–38
91. Dunlop BW, Rajendra JK, Craighead WE, et al: Functional connectivity of the subcallosal cingulate cortex and differential outcomes to treatment with cognitive-behavioral therapy or antidepressant medication for major depressive disorder. Am J Psychiatry 2017; 174:533–545
92. McGrath CL, Kelley ME, Holtzheimer PE, et al: Toward a neuroimaging treatment selection biomarker for major depressive disorder. JAMA Psychiatry 2013; 70:821–829
93. Cha J, Choi KS, Rajendra JK, et al: Whole brain network effects of subcallosal cingulate deep brain stimulation for treatment-resistant depression. Mol Psychiatry 2024; 29:112–120
94. Dunlop BW, Cha J, Choi KS, et al: Functional connectivity of salience and affective networks among remitted depressed patients predicts episode recurrence. Neuropsychopharmacology 2023; 48:1901–1909
95. Mayberg H: Dualism in the era of device interventions: recovery takes more than a stimulator. AJOB Neurosci 2014; 5:1–2

Data supplement for Song et al., Connectomic Determinants of Subcallosal Cingulate Deep Brain Stimulation for Depression. Am J Psychiatry (doi: 10.1176/appi.ajp.20250449)

TABLE S1. DBS amplitude in each cohort

Cohort	Current (s.d.) [mA]	Voltage (s.d.) [V]
C1	5.97 (1.78)	3.83 (1.25)
C2	7.48 (1.09)	-
C3	7.08 (1.02)	4.39 (0.65)
Mean	6.89 (1.49)	4.07 (1.05)

TABLE S2. Comparison of within-group spatial concentration of DBS target locations in each cohort

RES: Responder; NON: Non-responder.

Cohort	Hemisphere	RES (distance)	NON (distance)	Logistic			Linear		
				OR	95% CI	p uncorrected	β	95% CI	p uncorrected
C1	Left	4.90	5.85	0.18	[0.06, 0.50]	< 0.001	-14.48	[-19.95, 9.02]	< 0.001
	Right	5.09	5.68	0.62	[0.36, 1.06]	0.071	-6.40	[-13.14, 0.33]	0.062
C2	Left	4.78	7.68	0.12	[0.03, 0.44]	< 0.001	-15.04	[-20.12, -9.97]	< 0.001
	Right	3.58	6.73	0.02	[0.00, 0.27]	0.002	-17.47	[-25.53, -9.41]	< 0.001
C3	Left	4.39	6.85	0.41	[0.21, 0.81]	0.008	-5.06	[-9.48, -0.64	0.026
	Right	5.11	6.24	0.66	[0.35, 1.22]	0.167	-1.94	[-8.17, 4.29]	0.529

TABLE S3. Comparison of coordinates of DBS target locations in each cohort
RES: Responder; NON: Non-responder.

Cohort	Hemisphere	RES (x, y, z)	NON (x, y, z)	Hotelling's T^2	df1	df2	p uncorrect
C1	Left	(-9.5, 23.0, -11.0)	(-9.0, 22.5, -10.5)	2.458	3	46	0.509
	Right	(7.0, 23.0, -11.5)	(7.0, 23.0, -10.0)	1.736	3	46	0.648
C2	Left	(-7.5, 25.0, -8.5)	(-7.0, 25.5, -8.5)	2.407	3	46	0.518
	Right	(5.5, 25.0, -8.5)	(6.0, 26.5, -7.5)	2.284	3	46	0.541
C3	Left	(-8.0, 27.5, -8.0)	(-8.0, 28.5, -8.5)	1.281	3	33	0.753
	Right	(5.0, 27.5, -8.0)	(6.0, 27.0, -8.5)	2.147	3	33	0.575

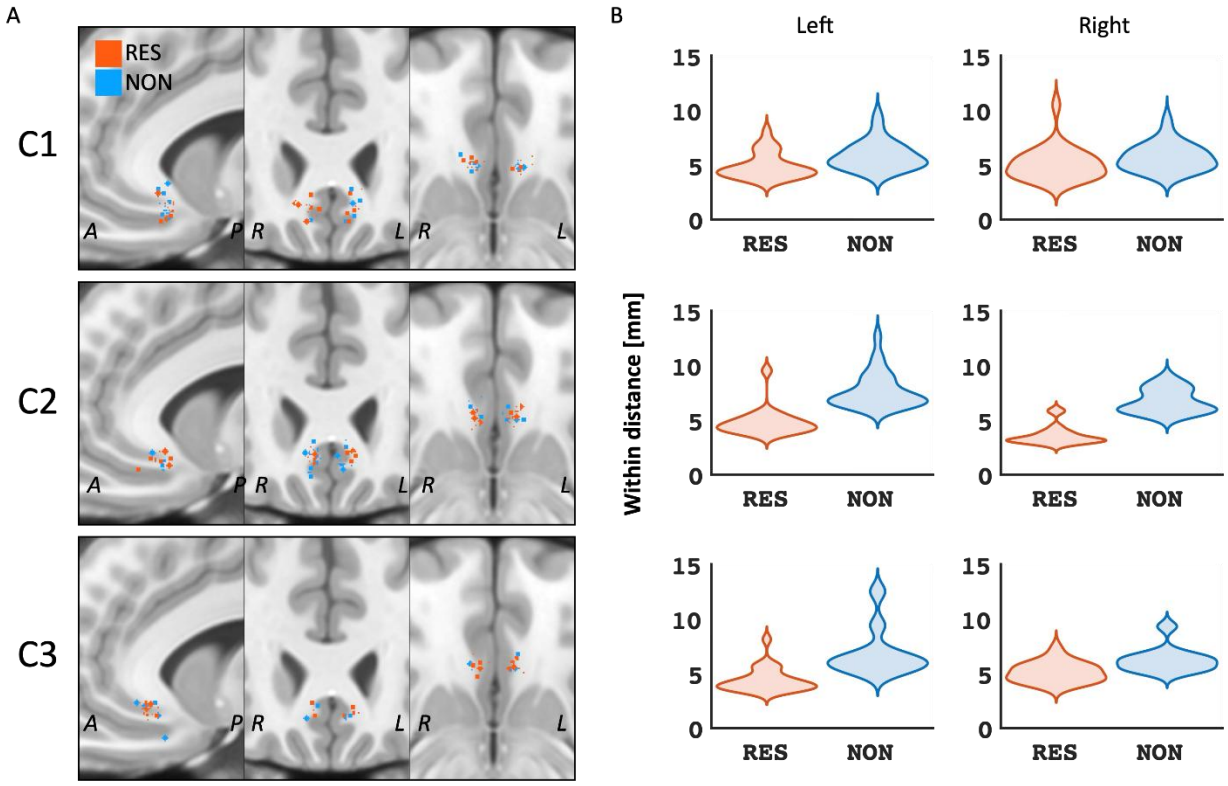
TABLE S4. Comparison of individual fiber activation in each cohort
CBL: Left cingulum bundle; CBR: Right cingulum bundle; FM: Forceps minor; mUFL: Left medial uncinate fasciculus; mUFR: Right medial uncinate fasciculus.

Cohort	Bundle	Logistic			Linear		
		OR	95% CI	p uncorrected	β	95% CI	p uncorrected
C1	CBL	1.001	[1.000, 1.002]	0.089	0.015	[0.001, 0.029]	0.033
	CBR	1.000	[0.994, 1.007]	0.979	0.009	[-0.009, 0.104]	0.845
	FM	1.000	[0.999, 1.000]	0.341	0.000	[-0.002, 0.000]	0.167
	mUFL	1.009	[1.001, 1.017]	0.018	0.089	[0.029, 0.150]	0.005
	mUFR	1.017	[0.978, 1.059]	0.379	0.323	[-0.199, 0.844]	0.219
C2	CBL	1.002	[1.001, 1.003]	0.004	0.023	[0.011, 0.034]	< 0.001
	CBR	1.004	[0.997, 1.012]	0.207	0.081	[-0.029, 0.191]	0.144
	FM	1.000	[1.000, 1.001]	0.786	0.000	[-0.001, 0.000]	0.814
	mUFL	1.037	[1.010, 1.065]	0.006	0.174	[0.116, 0.233]	< 0.001
	mUFR	1.073	[0.976, 1.179]	0.132	1.203	[0.180, 2.227]	0.022
C3	CBL	1.001	[1.000, 1.003	0.084	0.007	[-0.004, 0.018]	0.217
	CBR	1.001	[0.998, 1.018]	0.123	0.061	[-0.026, 0.148]	0.162
	FM	1.000	[1.000, 1.000]	0.653	0.000	[0.000, 0.001]	0.250
	mUFL	1.006	[0.997, 1.015]	0.201	0.030	[-0.052, 0.112]	0.460
	mUFR	0.976	[0.899, 1.059]	0.537	-0.372	[-1.167, 0.423]	0.347

TABLE S5. Comparison of 10-fold cross-validated performance metrics across different combinations of WM bundles included in fiber-PSM regression models

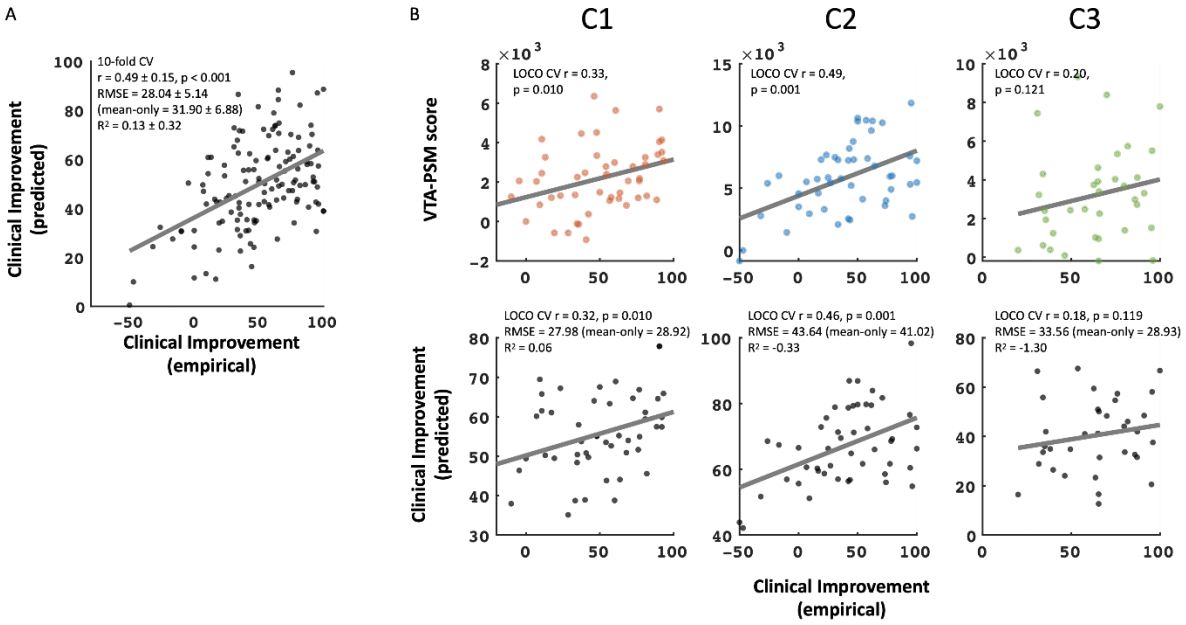
WM	R^2	RMSE	mean-only RMSE
CBL + CBR + FM + mUFL + mUFR	0.04 ± 0.23	30.01 ± 6.50	
CBL + CBR + mUFL + mUFR	0.23 ± 0.19	26.77 ± 5.74	
CBL + mUFL	0.23 ± 0.20	26.70 ± 5.73	
CBR + mUFR	0.03 ± 0.25	30.11 ± 7.00	
CBL	0.22 ± 0.17	26.94 ± 5.82	31.90 ± 6.88
CBR	0.02 ± 0.24	30.26 ± 6.91	
FM	-0.02 ± 0.25	30.89 ± 6.79	
mUFL	0.17 ± 0.30	27.29 ± 5.28	
mUFR	0.01 ± 0.26	30.53 ± 7.53	

FIGURE S1. Cohort-specific comparison of DBS target locations
A. Distributions of DBS target locations for responders and non-responders. **B.** Within-group spatial distance (mm) of DBS target locations in the bilateral hemispheres.



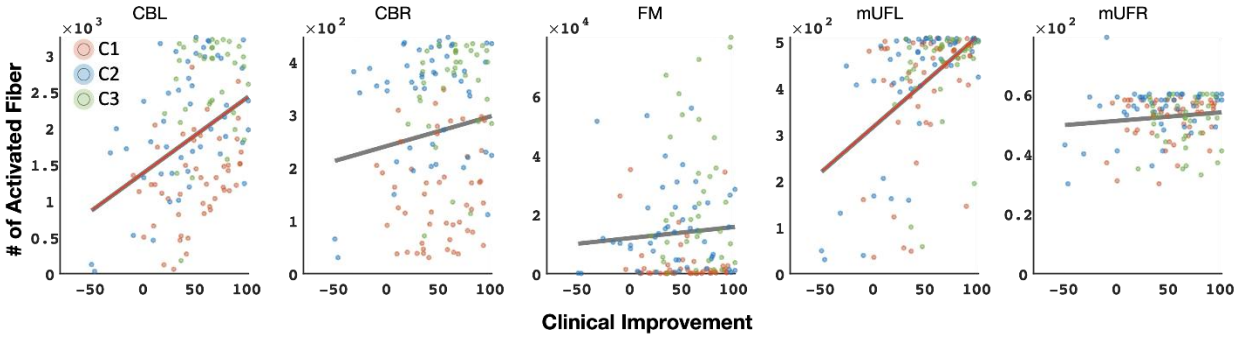
Alt text: Two-panel figure showing cohort-specific distributions of DBS target locations for responders and non-responders, along with comparisons of within-group spatial distances across hemispheres.

FIGURE S2. Cross-validation analyses based on the VTA-PSM score
A. In 10-fold cross-validation, linear associations between empirical and predicted clinical improvement in held-out data, with corresponding cross-validated performance metrics. **B.** In leave-one-cohort-out cross-validation, linear associations between empirical clinical improvement and VTA-PSM score in held-out cohorts (top), and between empirical and predicted clinical improvements in held-out cohorts (bottom).



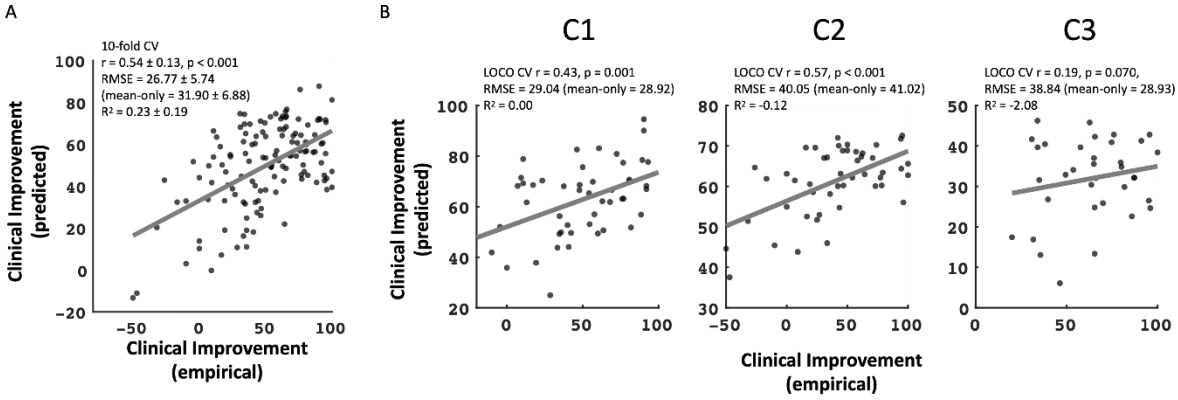
Alt text: Two-panel figure showing cross-validation analyses based on the VTA-PSM score, including associations between empirical and predicted clinical improvement in 10-fold and LOCO analyses and associations between empirical clinical improvement and VTA-PSM score in LOCO analyses.

FIGURE S3. Linear associations between clinical improvement and the number of activated fibers
Dots are colored according to cohort. Red fitted lines indicate significant linear associations.



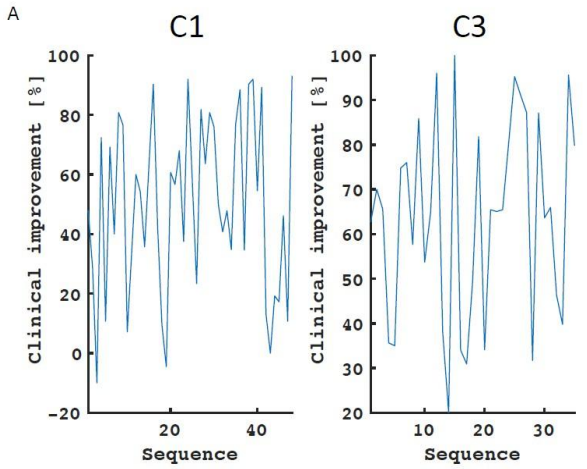
Alt text: Scatter plots showing linear relationships between clinical improvement and the number of activated WM fibers, with data points colored by cohort and fitted lines.

FIGURE S4. Cross-validation analyses based on the summed fiber-PSM score
Linear associations between empirical and predicted clinical improvements in held-out data, with corresponding cross-validated performance metrics, shown for 10-fold cross-validation (**A**) and LOCO cross-validation (**B**).



Alt text: Two-panel figure showing cross-validation analyses based on the summed fiber-PSM score, including scatter plots of empirical versus predicted clinical improvement in held-out data for 10-fold and LOCO cross-validation analyses, with fitted lines.

FIGURE S5. Temporal effects on clinical improvement in single-site cohorts (C1 and C3)



B

		Without time regressor		With time regressor	
Cohort	WM	AIC	BIC	AIC	BIC
C1	CB	459.96	469.31	461.73	472.96
	mUF	456.17	465.53	458.02	469.25
C3	CB	321.31	329.08	321.86	331.19
	mUF	322.47	330.24	323.24	332.57

A. Clinical improvement plotted across the temporal sequence of DBS implantation in C1 (left) and C3 (right). **B.** AIC and BIC comparisons for models with and without a temporal sequence regressor in each cohort. In both C1 and C3, inclusion of the sequence regressor did not indicate improved model fit.

Alt text: Two-panel figure showing clinical improvement plotted by implantation sequence in single-site cohorts C1 and C3, and model comparison results using AIC and BIC for models with and without a temporal sequence regressor.